Fast Efficiency Optimization Control Based on Orthogonal Current Phasor Model for Linear Oscillatory Motor

Wei Xu, *Fellow, IEEE*, Yifan Gong, Jian Ge, *Member, IEEE*, Kaiju Liao, Guangyu Liao, Maoxin Zhang, and Ion Boldea, *Life Fellow, IEEE*

***Abstract*—As the key power part of the linear compressor, the linear oscillatory motor (LOM) has been paid more attention by both academia and industry recently for its compact size, high efficiency, low vibration, etc. In practice, the efficiency of LOM is significantly impacted by the changes in load parameters, of which the best working point can be tracked by the resonant frequency tracking control (RFTC). However, the traditional RFTC with the idea of stroke-current phase suffers some problems, such as slow tracking speed, low accuracy, fluctuate amplitude of piston, and so on. In this article, a novel fast efficiency optimization control algorithm based on the orthogonal current phasor model is proposed for LOM. This new model can achieve the decoupling of current components that act on piston stroke and system efficiency, respectively. Moreover, the driving frequency can be adjusted by current decoupling control with a designed phase-locked loop. Based on the aforementioned, the decoupling control of the LOM drive system can be achieved, which can simultaneously improve the system response speed and the output efficiency. Comprehensive simulation and experimental results have fully demonstrated the advantages of the proposed method.**

***Index Terms*—Efficiency optimization control, linear compressor, linear oscillatory motor (LOM), orthogonal current phasor model, resonant frequency tracking control (RFTC).**

Manuscript received 16 January 2024; revised 2 May 2024; accepted 31 May 2024. Date of publication 11 June 2024; date of current version 16 July 2024. This work was supported in part by the National Natural Science Foundation of China under Grant 52277050, in part by the Shenzhen International Cooperation Research Project under Grant GJHZ20210705142539007, and in part by the Natural Science Foundation of Shenzhen Municipality under Grant JCYJ20230807143701003. Recommended for publication by Associate Editor J. Ye. *(Corresponding author: Jian Ge.)*

Wei Xu and Kaiju Liao are with the State Key Laboratory of Advanced Electromagnetic Technology, Huazhong University of Science and Technology, Wuhan 430074, China, and also with the Key Laboratory of High Density Electromagnetic Power and Systems, Institute of Electrical Engineering, Chinese Academy of Sciences, Beijing 100190, China (e-mail: weixu@mail.iee.ac.cn; kaijuliao@mail.iee.ac.cn).

Yifan Gong, Jian Ge, Guangyu Liao, and Maoxin Zhang are with the State Key Laboratory of Advanced Electromagnetic Technology, Huazhong University of Science and Technology, Wuhan 430074, China (e-mail: yifangong@hust.edu.cn; gejian1994@hust.edu.cn; gyliao@hust.edu.cn; maoxin23@hust.edu.cn).

Ion Boldea is with the Romanian Academy-Timisoara Branch, 300223 Timisoara, Romania, and also with the Politehnica University Timisoara, 300006 Timisoara, Romania (e-mail: ion.boldea@upt.ro).

Color versions of one or more figures in this article are available at https://doi.org/10.1109/TPEL.2024.3412739.

Digital Object Identifier 10.1109/TPEL.2024.3412739

I. Introduction

As THE core part of refrigeration equipment, such as refrigerator and air conditioning, the linear compressor has higher efficiency, lower noise and vibration, smaller volume, etc., compared to the traditional rotary compressor [1], [2], [3]. For its direct-drive manner, the linear compressor system can successfully remove the mechanical transmission components, such as crankshaft and connecting rod, which can reduce the energy loss of the intermediate link greatly [4], [5]. In general, the efficiency of linear compressor is 15%–25% higher than that of traditional rotary compressor, where the key power component, linear oscillatory motor (LOM), can usually get high efficiency with over 90% [6], [7], [8].

In general, the working efficiency of linear compressor changes with the variation of driving frequency and gas load parameters. For a particular gas load, the linear compressor can work at the highest efficiency by adjusting the working frequency approaching to the resonant frequency [9]. When the operating frequency is far away from the resonant operating point, the efficiency of LOM will be seriously reduced. Therefore, the efficiency optimization control strategies should be carried out to ensure the efficient operation of linear compressor.

In the early stage, the constant frequency control is adopted for the LOM, which leads to an inefficient operation since the characteristics of the motor are neglected. Then, a double closed-loop control method of stroke and frequency is proposed, which makes the LOM work close to its mechanical resonance frequency [9]. Such control strategy has become the mainstream control scheme for LOM in the following researches. Subsequently, a control strategy based on zero crossing detection is proposed to obtain the mechanical resonance frequency, which is easy to implement [10]. However, it has suffered a series of defects, such as being sensitive to noise and vibration.

To get around such problem, a phase angle detection method based on the average value of stroke-current product (ASCP) is proposed [11]. It points out that the phase difference between piston stroke and current is 90° when the LOM operates at its resonant frequency. And the drive frequency can be adjusted to the resonant frequency according to the stroke-current phase difference, which realizes the efficient operation. Inspired by this idea, the follow-up studies have been mostly focused on the method to obtain the stroke-current phase difference. Different judgment

criteria are used to identify the resonant frequency of the motor, and the given frequency of sinusoidal pulse width modulation (SPWM) is modified to achieve the tracking effect. Therein, a resonant frequency tracking control (RFTC) algorithm for the LOM based on virtual coordinates and second-order generalized integrator is proposed [12]. The phase difference information of current and piston stroke is obtained by coordinate transformation and calculation of current. This scheme of tracking the resonant frequency can accurately follow the optimal working frequency of the motor and effectively improve the operation efficiency of LOM. However, the idea of this algorithm is still limited to calculating the phase difference between piston stroke and current, which obtains the resonant frequency indirectly. The calculation of the phase difference will be affected by the dynamic operation of the motor, thus reducing the response speed of the frequency following when the motor starts, changes the piston amplitude, and changes the load. Meanwhile, this control strategy is dependent on the relationship between phase difference of stroke-current and resonant frequency, which is mostly based on qualitative analysis without strict mathematical derivation and analysis.

In order to get rid of the limitation of indirectly calculating the resonant frequency through the phase difference of piston stroke and current, the method of parameter identification is used to realize resonance frequency tracking in [13] and [14]. The RFTC based on model reference adaptive system is proposed in [13], and another control strategy via adaptive full-order observer is proposed in [14]. Aiming at identifying gas load parameters of the LOM system to calculate the resonance frequency directly, these two methods have better tracking ability when the working state of the motor changes. However, there are still some problems in its convergence speed and stability of parameter identification. Meanwhile, the idea is still to identify and then track the resonant frequency, which still suffers from the problem of slow response for RFTC.

For the control strategies mentioned earlier, the efficiency control and the piston stroke control cannot be decoupled. It is known that the current control can reach a faster response than the V-F control. However, as a single-phase motor, it is difficult to achieve current control for LOM. Due to the use of three-phase current and related space vectors for coordinate transformation, the conventional dq-axis decoupled vector control cannot be used for the LOM directly. As a result, the abovementioned control schemes adopt a similar V-F control method with directly given voltage and frequency. Meanwhile, compared to traditional single-phase motor, LOM has the characteristic of highly coupled system, which lead to a slower response of the system. To get around this problem, the amplitude detection is used to achieve the current control for LOM [15], [16]. Nevertheless, such methods cannot get real-time current information, and the control result is not satisfied enough.

In order to solve the abovementioned problems, a novel fast efficiency optimization control method is proposed for LOM based on an orthogonal current phasor model. The main contributions of this article can be summarized as follows.

1) Based on the idea of virtual coordinate system, an orthogonal current phasor model is designed for LOM. The complexity and coupling degree of the motor model are reduced effectively by decomposition of current phasor. And by analyzing the relationship between the current component in the direction of velocity and piston stroke, the LOM system is decomposed into two decoupled parts to achieve independent control of its amplitude and frequency.
2) The current decoupling control (CDC) is proposed based on the orthogonal current phasor model. By keeping the current component orthogonal to the velocity to zero, the function of efficiency optimization control can be achieved. By controlling the current component in phase with speed, the response speed of the piston stroke control can be improved with the current closed-loop.
3) The signal processing strategy is specially designed for the current orthogonal model and decoupling control concept mentioned earlier. The SOGI-QSG and phase-locked loop (PLL) are used to process the voltage and current signals. The relevant orthogonal signals are obtained by a SOGI-QSG while filtering and further achieves the observation of piston stroke, and a single-phase PLL is used to obtain the frequency and phase information as required in the transformation.

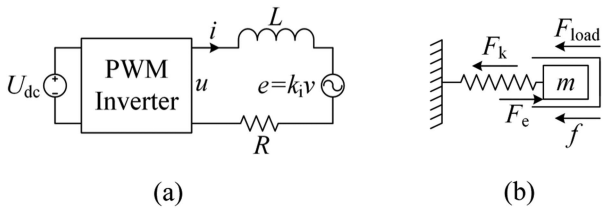

Fig. 1. Basic model of the LOM. (a) Equivalent circuit. (b) Kinetics model.

The rest of this article is organized as follows. In Section II, the mathematical model of LOM is introduced and the system characteristic is analyzed to show the control principle of traditional RFTC. In Section III, the orthogonal current phasor model and CDC are proposed. In Section IV, the signal processing and position calculation used for CDC are illustrated in detail. In Section V, the proposed algorithm is verified by comprehensive simulation and experimental results. Finally, conclusions are drawn in Section VI.

II. Mathematical Model and System Characteristic Analysis

A. Mathematical Model of the LOM

The structure of LOM is shown in Fig. 1. In order to simplify the analysis, the following assumptions are given: 1) Core saturation is neglected; 2) Eddy current and hysteresis loss are ignored; 3) Gas load force is linear.

As shown in Fig. 1(a), the circuit equation of LOM can be expressed as follows:

$$u = Ri + L\frac{di}{dt} + e \tag{1}$$

where u is the input voltage supplied by a PWM inverter with bus voltage U_{dc}, i the current, R the winding resistance, L the winding inductance, and e the back electromotive force (EMF) generated by the movement of mover. The back EMF is proportional to the velocity v with a structure-based coefficient k_{i}, as given by

$$e = \frac{d\psi_{\mathrm{m}}}{dt} = \frac{d\psi_{\mathrm{m}}}{dx} \cdot \frac{dx}{dt} = k_i v \tag{2}$$

where ψ_{m} is the permanent magnet flux and x the piston stroke.

In the kinetics model as Fig. 1(b), the electromagnetic thrust F_{e} is also proportional to the current with k_{i}, which is given as follows:

$$F_{\mathrm{e}} = k_{\mathrm{i}} i = F_{\mathrm{k}} + F_{\mathrm{load}} + f = m\frac{d^2x}{dt^2} + c\frac{dx}{dt} + kx \tag{3}$$

where F_{k} is the string force, F_{load} the load force, f the friction force, m the total mass of mover and piston, k the equivalent elastic coefficient of the system, and c the equivalent friction coefficient of the system.

B. Analysis of System Characteristic

Since the linear compressor is driven by single-phase alternating current (ac), the mathematical model can be written in phasor form, as illustrated by

$$\begin{cases} \dot{U} = \dot{I}\left(R + j\omega L\right) + k_{\mathrm{i}}\dot{V} \\ k_{\mathrm{i}}\dot{I} = \left[c + j\left(\omega m - \frac{k}{\omega}\right)\right]\dot{V} \end{cases} \tag{4}$$

By calculating the input and output power of the system, the efficiency of the motor can be obtained by

$$\eta = \frac{P_{\mathrm{out}}}{P_{\mathrm{in}}} = \frac{\mathrm{Re}\left(\dot{U}\dot{I}\right)}{\mathrm{Re}\left(\dot{F}\dot{V}\right)} = \frac{{k_{\mathrm{i}}}^2 c}{{k_{\mathrm{i}}}^2 c + R_{\mathrm{e}}\left({R_{\mathrm{m}}}^2 + {X_{\mathrm{m}}}^2\right)} \tag{5}$$

where the equivalent mechanical impedance is given by

$$Z_{\mathrm{m}} = R_{\mathrm{m}} + jX_{\mathrm{m}} = c + j\left(m\omega - \frac{k}{\omega}\right). \tag{6}$$

As seen from (5), X_{m} is the only parameter changing with the driving frequency, and when the load of the compressor is determined, the other parameters are fixed values. That is to say, the working efficiency of the motor under the same working condition is only related to the driving frequency. When X_{m} in the equivalent mechanical impedance is 0, the system efficiency has the maximum value. From (6), it can get the driving frequency $\omega = \sqrt{K/m} = \omega_0$, that is, when the input voltage frequency is equal to the system resonant frequency, the compressor has the highest working efficiency.

In order to determine the relationship between the observed current, piston stroke and working efficiency of the system, the relationship between piston stroke and current can be expressed as follows:

$$\frac{\dot{X}}{\dot{I}} = \frac{k_{\mathrm{i}}}{j\left(R_{\mathrm{m}} - X_{\mathrm{m}}\right)\omega} \tag{7}$$

$$\theta_{x-i} = -\arctan\left(\frac{c\omega}{k - m\omega^2}\right). \tag{8}$$

When the system reaches its highest efficiency, X_{m} in the equivalent mechanical impedance is 0. At this time, it can be seen that the phase angle between the piston stroke and current is $-90°$, i.e., the current is 90° ahead of the piston stroke. The analysis shows that there is a monotonic relationship between the driving frequency and the phase angle (between piston stroke and current). Taking this as the judgment criterion, the frequency closed-loop control of LOM is carried out by calculating the trigonometric function value of the phase angle.

III. Orthogonal Current Phasor Model of LOM and CDC

The traditional LOM model can effectively analyze the system characteristics, which is usually used for frequency and amplitude control. However, compared to other traditional single-phase motors, the physical quantities in this model are highly coupled, so it is hard to get good control performance. Meanwhile, due to the lack of analysis of the current model, control strategies based on traditional models could only use single-phase sinusoidal current signals. Although some control techniques such as PR/PIR can be used to control the ac, the control performance is unsatisfied under high-frequency operating conditions. Therefore, it is necessary to analyze the current model of LOM.

A. Orthogonal Current Phasor Model of LOM

When the LOM operates at steady state, the phase difference between electromagnetic thrust and piston velocity can be derived as follows:

$$\theta_{\mathrm{v-Fe}} = \theta_{\mathrm{v-i}} = \arctan\left(\frac{m\omega^2 - k}{c\omega}\right) \tag{9}$$

where ω is the angular frequency.

Thus, the current can be decomposed into the component I_{v} in phase with the velocity and the component I_{x} orthogonal to the velocity. The phaser equation can be described by

$$\begin{cases} \dot{U} = \left(\dot{I}_{\mathrm{v}} + \dot{I}_{\mathrm{x}}\right)\left(R + j\omega L\right) + k_{\mathrm{i}}\dot{V} \\ \dot{I}_{\mathrm{v}} + \dot{I}_{\mathrm{v}} = \dot{I} \\ k_{\mathrm{i}}\left(\dot{I}_{\mathrm{v}} + \dot{I}_{\mathrm{x}}\right) = \left(R_{\mathrm{m}} + jX_{\mathrm{m}}\right)\dot{V} \end{cases} \tag{10}$$

where the equivalent mechanical impedance is given by

$$Z_{\mathrm{m}} = R_{\mathrm{m}} + jX_{\mathrm{m}} = c + j\left(m\omega - \frac{k}{\omega}\right). \tag{11}$$

According to the phase relationship between $\dot{I}_{\mathrm{v}}$, $\dot{I}_{\mathrm{x}}$ and $\dot{V}$, the expressions of the two current components can be described as follows:

$$\begin{bmatrix} \dot{I}_{\mathrm{v}} \\ \dot{I}_{\mathrm{x}} \end{bmatrix} = \frac{\dot{I}}{R_{\mathrm{m}} + jX_{\mathrm{m}}} \begin{bmatrix} R_{\mathrm{m}} \\ jX_{\mathrm{m}} \end{bmatrix}. \tag{12}$$

The corresponding phasor diagram can be obtained in Fig. 2.

Furthermore, the expression of velocity and piston stroke with respect to the two current components is

$$\dot{V} = \frac{k_{\mathrm{i}}\dot{I}_{\mathrm{v}}}{R_{\mathrm{m}}}, \dot{X} = -\frac{jk_{\mathrm{i}}\dot{I}_{\mathrm{v}}}{\omega R_{\mathrm{m}}}. \tag{13}$$

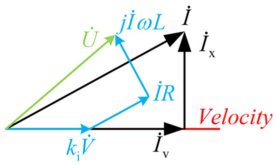

Fig. 2. Phasor diagram of the LOM.

The amplitude of both velocity and piston stroke is proportional to the current component $\dot{I}_v$. In this way, the motion equation of LOM presents a linear function relationship similar to that of direct current (dc) motor.

B. Relation Between Efficiency and Current Phasor

The expressions of input and output power derived from orthogonal current vector model can be expressed as follows:

$$\begin{cases} P_{in} = \mathrm{Re}\left(\dot{U}\bar{\dot{I}}\right) = \left(R + \frac{k_i^2}{R_m}\right)\left|\dot{I}_v\right|^2 + R_e\left|\dot{I}_x\right|^2 \\ P_{out} = \mathrm{Re}\left(\dot{F}_e\bar{\dot{V}}\right) = \frac{k_i^2}{R_m}\left|\dot{I}_v\right|^2 \end{cases} \tag{14}$$

where the output power is proportional to the square of the current component $\dot{I}_v$, while the input power is determined by the square of both current components. The efficiency expression of the motor can be obtained as follows:

$$\eta_e = \frac{P_{out1}}{P_{in}} = 1 - \frac{RR_m\left|\dot{I}\right|^2}{\left(RR_m + k_i^2\right)\left|\dot{I}\right|^2 - k_i^2\left|\dot{I}_x\right|^2}. \tag{15}$$

According to (15), it can be known that when the input current is constant, the efficiency will be affected by the amplitude of current component $\dot{I}_x$. And the maximum of efficiency can be achieved when $\dot{I}_x = 0$. At this time, the current and piston velocity are in the same phase. In addition, the piston motion is proportional to the current component $\dot{I}_v$. Therefore, the piston stroke can be adjusted by controlling the value of $\dot{I}_v$.

The relationship among the current component I_x, the phase between piston stroke and current, and the system driving frequency can be further calculated by

$$I_x = I_m \cos\theta_{x-i} = \frac{I_m\left(m\omega^2 - k\right)}{\sqrt{m^2\omega^4 + \left(c^2 - 2mk\right)\omega^2 + k^2}} \tag{16}$$

where I_m is the amplitude of current. It is noted that the current component I_x is essentially related to the phase difference between piston stroke and current. Using the motor data of the experimental platform, the ratio of I_x to I_m is plotted as shown in Fig. 3.

The I_x increases monotonously with the motor drive frequency, and when the motor operates at its resonant frequency, i.e., $\omega = \omega_0 = \sqrt{k/m}$, the current component $I_x = 0$. Therefore, this control method performs as an RFTC algorithm in principle. And the response speed of frequency tracking can be effectively improved by avoiding the definite integral calculation in traditional RFTC algorithm.

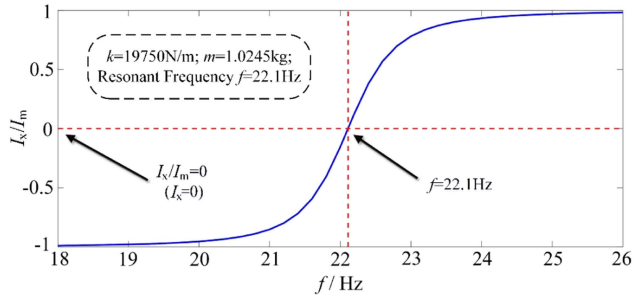

Fig. 3. Relation between the ratio of current component I_x and current amplitude I_m and driving frequency f.

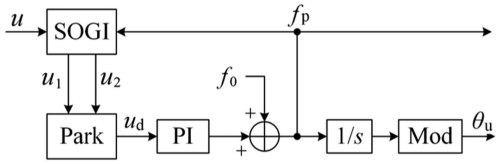

Fig. 4. Control block diagram of the PLL.

C. Current Decoupling Control

The current loop control method of LOM is different from that of traditional motors, and its origin lies in the following two points: 1. The electrical angle acquisition of coordinate transformation; 2. Adjustment of drive frequency. It is not only necessary to obtain the frequency and phase of the system, but also to achieve the effect of frequency regulation by controlling the current component. Therefore, LOM needs to analyze its frequency and phase control scheme separately, as detailed in the following.

Based on the designed orthogonal current phasor model, the two current components can be adjusted, respectively. Different from the general ac motor, the position signal of LOM is sinusoidal and has a phase difference with its voltage signal. According to (1), (2), and (9), this phase difference can be obtained as follows:

$$\theta_{u-x} = \arctan\left(\frac{RR_m + k_i^2 - \omega LX_m}{RX_m + \omega LR_m}\right). \tag{17}$$

The angle θ_{u-x} is related to the equivalent mechanical impedance $Z_m = R_m + jX_m$ which changes constantly during motor operation and it is impossible to get their real-time values. On the other hand, the phase of position signal cannot be directly extracted due to the varying amplitude. Therefore, the position signal cannot be directly used for Inv. Park Trans.

According to the abovementioned problem, a PLL should be applied for the voltage control of LOM, whose control block diagram is shown in Fig. 4. The voltage angle obtained by the PLL can be used for Inv. Park Trans. to generate the fundamental voltage signal, thus completing the closed loop of CDC [17].

The "Mod" in Fig. 4 refers to the residual calculation, aimed at obtaining the electrical angle within the range. The "f_0" refers to the initial reference frequency input in PLL, which is used to promote the response speed and tracking ability for PLL. Moreover, the PLL not only provides the angle of vector control,

but also plays an important role of frequency regulation. For general ac motors, the speed and driving frequency can be adjusted by increasing or decreasing the torque current component. However, the electromagnetic thrust of LOM is independent of the driving frequency. Simply adjusting the electromagnetic thrust will only change the motion stroke of the piston, but not the operating frequency of the system.

Therefore, the LOM control system needs a special frequency regulation part. The traditional control scheme adopts the method of directly setting the frequency of the voltage for frequency modulation, while the control of $I_{\mathrm{x}} = 0$ and voltage PLL in this control method accomplish this work together.

The current controller is in the form of PI. The outputs of the two controllers are, respectively, recorded as ${u_{\mathrm{v}}}^*$ and ${u_{\mathrm{x}}}^*$, which can be described as follows:

$$\begin{cases} u_{\mathrm{v}}^*(t) = K_{\mathrm{p1}} e_{\mathrm{iv}}(t) + K_{\mathrm{i1}} \int_{t_0}^{t} e_{\mathrm{iv}}(\tau)\, d\tau \\ u_{\mathrm{x}}^*(t) = K_{\mathrm{p2}} e_{\mathrm{ix}}(t) + K_{\mathrm{i2}} \int_{t_0}^{t} e_{\mathrm{ix}}(\tau)\, d\tau \end{cases} \tag{18}$$

where K_{p1} and K_{i1} represent the proportional control gain and the integral control gain of ${u_{\mathrm{v}}}^*$, K_{p2} and K_{i2} represent the proportional control gain and the integral control gain of ${u_{\mathrm{x}}}^*$. The errors of the two current component controllers are $e_{\mathrm{iv}} = {I_{\mathrm{v}}}^* - I_{\mathrm{v}}$ and $e_{\mathrm{ix}} = -I_{\mathrm{x}}$, respectively, where ${I_{\mathrm{v}}}^*$ is the given value of current component I_{v}.

According to Inv. Park Trans. and the characteristics of SOGI, the expressions of two voltage signals output by SOGI can be obtained as follows:

$$\begin{cases} \hat{u}_1 = u_{\mathrm{v}}^*(t)\cos\theta_{\mathrm{U}} + u_{\mathrm{x}}^*(t)\sin\theta_{\mathrm{U}} \\ \hat{u}_2 = -u_{\mathrm{v}}^*(t)\sin\theta_{\mathrm{U}} + u_{\mathrm{x}}^*(t)\cos\theta_{\mathrm{U}} \end{cases} \tag{19}$$

where θ_{U} is the angle of the voltage signal. Furthermore, the error of PI controller in voltage PLL can be obtained as follows:

$$\begin{aligned} e_{\mathrm{PLL}}(t) &= u_{\mathrm{x}} = u_1 \sin\theta_{\mathrm{U}} + u_2 \cos\theta_{\mathrm{U}} = u_x^*(t) \\ &= -K_{\mathrm{p2}} I_{\mathrm{x}}(t) - K_{\mathrm{i2}} \int_{t_0}^{t} I_{\mathrm{x}}(\tau)\, d\tau. \end{aligned} \tag{20}$$

Similarly, the controller of the PLL is also in the form of proportional integral (PI). Its output frequency f_{p} can be expressed as follows:

$$f_{\mathrm{p}}(t) = f_0 + K_{\mathrm{pf}} e_{\mathrm{PLL}}(t) + K_{\mathrm{if}} \int_{t_0}^{t} e_{\mathrm{PLL}}(\tau)\, d\tau \tag{21}$$

where K_{pf} and K_{if} represent the proportional control gain and the integral control gain of ${f_{\mathrm{p}}}^*$. The relationship between current component I_{x} and frequency obtained in Section II-B is shown in (16). As shown in (16), (20), and (21), it is the adjustment mode of motor drive frequency under the internal and external PI controllers.

In conclusion, this control method realizes the adjustment of piston amplitude through the double closed loop control of amplitude $-I_{\mathrm{v}}$, and the tracking of resonance frequency through the double closed loop control of $I_{\mathrm{x}} -$ PLL. Compared with the traditional control algorithm, this scheme adds a complete current loop, which can effectively improve the response speed of various performance.

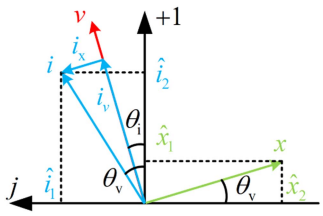

Fig. 5. Phasor diagram of current, velocity, and piston stroke.

IV. Signal Processing and Position Calculation

As a single-phase motor, the current and voltage of LOM are single-phase sine signal, which cannot be used for coordinate transformation directly or through basic Clark/Park Trans. Meanwhile, the traditional position estimation algorithm also has some issues such as integral drift. Therefore, the signal processing and position estimation algorithm of LOM need to be further investigated.

A. Signal Processing Method

The current and position signals need to be calculated to achieve the current control as described in Section II. Meanwhile, there are also interference problems such as dc component and high-frequency noise in current sampling. Therefore, one effective processing method of voltage, current, and position signals is designed for LOM.

As a good orthogonal signal generator, the second-order SOGI based quadrature signal generator (SO-SOGI-QSG) is widely used in grid-connected inverter [18]. Both output channels have adaptive band-pass filtering effect while orthogonal processing is performed on the signal [19]. Through the SO-SOGI-QSG processing, the dc component and noise interference in the signal can be effectively filtered, thus improving the accuracy of signal calculation. SO-SOGI-QSG can be used to process the signal to obtain the filtered signal and its orthogonal signal, so as to complete the subsequent calculation.

The transient state of the motor during operation is taken for analysis. It assumes that the phase angle of the piston velocity signal is θ_{v}, then the velocity amplitude is v_{m}, and the phase angle of the current signal is θ_{i}, that is to say, $v = v_{\mathrm{m}} \sin\theta_{\mathrm{v}}$, $i = i_{\mathrm{m}} \sin\theta_{\mathrm{i}}$. According to the integral relationship between velocity and piston stroke, the two processed piston stroke signals $\hat{x}_1, \hat{x}_2$ and two current signals $\hat{i}_1, \hat{i}_2$ can be expressed as follows:

$$\begin{bmatrix} \hat{x}_1 \\ \hat{x}_2 \end{bmatrix} = x_{\mathrm{m}} \begin{bmatrix} -\cos\theta_{\mathrm{v}} \\ \sin\theta_{\mathrm{v}} \end{bmatrix}, \quad \begin{bmatrix} \hat{i}_1 \\ \hat{i}_2 \end{bmatrix} = i_{\mathrm{m}} \begin{bmatrix} \sin\theta_{\mathrm{i}} \\ \cos\theta_{\mathrm{i}} \end{bmatrix} \tag{22}$$

where, x_{m} is the amplitude of piston stroke signal, and i_{m} is the amplitude of current signal. The sine and cosine of the phase angle of the piston velocity signal under this transient state can be obtained from (22), as illustrated by

$$\begin{bmatrix} \cos\theta_{\mathrm{v}} \\ \sin\theta_{\mathrm{v}} \end{bmatrix} = \frac{1}{\sqrt{\hat{x}_1^2 + \hat{x}_2^2}} \begin{bmatrix} -\hat{x}_1 \\ \hat{x}_2 \end{bmatrix}. \tag{23}$$

The phasor diagram of current, velocity, and piston stroke under this transient state is as shown in Fig. 5.

From the relationship, as shown in Fig. 5, the two current components, I_v and I_x as described in Section II, can be obtained through Park Trans., as given by

$$\begin{bmatrix} I_v \\ I_x \end{bmatrix} = \hat{i}_1 \begin{bmatrix} -\sin\theta_v \\ \cos\theta_v \end{bmatrix} + \hat{i}_2 \begin{bmatrix} \cos\theta_v \\ \sin\theta_v \end{bmatrix}. \tag{24}$$

The coordinate transformation of current is completed as shown in (24). The dc signals I_v and I_x in the rotating coordinate system with the velocity direction as the axis can be obtained by transformation from the sinusoidal signals $\hat{i}_1$ and $\hat{i}_2$ in the stationary coordinate system. Then, as analyzed in Sections II-B and II-C, the resonant frequency tracking and piston stroke control of LOM can be realized by adjusting the current components I_v and I_x.

For the amplitude calculation of piston motion, the traditional control algorithm mostly uses the amplitude detection algorithm. In this control program, the maximum and minimum values of the position signal are constantly detected, and the amplitude information can be calculated. The algorithm is easily interfered by the burr in the position signal, which can only complete one information update in a motion cycle, so as to deteriorate its dynamics and position accuracy. Therefore, a real-time calculation method of piston amplitude in this article can be obtained from (22), as described by

$$\hat{x}_m = \sqrt{\hat{x}_1^2 + \hat{x}_2^2}. \tag{25}$$

Because the piston is located in a forced vibration system composed of a mover and a spring, the motion waveform of the piston cannot abrupt under the motion inertia of the system. Therefore, the amplitude information of the piston can be calculated by using the orthogonal signal of piston stroke. This new method can update the amplitude information of the piston in each interruption cycle of the control program, which has a faster dynamic response than that of the traditional amplitude detection program.

B. Improved Method of Position Calculation

For the LOM, the most common sensorless control method is to directly calculate the piston position signal using the electrodynamic equation. The piston stroke x of the piston can be expressed as follows:

$$\hat{x} = \frac{1}{k_i}\int\left(u - Ri - L\frac{di}{dt}\right)dt = \frac{\int e dt}{k_i}. \tag{26}$$

It can be seen from (26) that a pure integration link exists in the calculation process of piston stroke, which would bring some problems of the initial value of integration and the integral drift. The improvement of position calculation method focuses on solving the problems caused by pure integration. The SO-SOGI-QSG as described in Section III-A is used to obtain filtered voltage and current signals, and their orthogonal signals, namely u_1, i_1 and u_2, i_2. According to the characteristics of SOGI, it can divide u_2 and i_2 by the angular speed of the motor, respectively, to obtain the integral of voltage and current versus time.

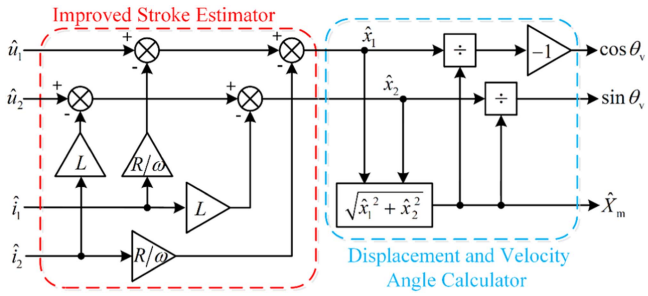

Fig. 6. Control block diagram of stroke estimator and signal calculator.

TABLE I
MAIN PARAMETERS OF THE LOM

Items	Value	Unit
Stator resistance, R	18.4	Ω
Stator inductance, L	0.755	H
Thrust constant, k_i	28.0	N/A
Spring coefficient, k	22.3	kN/m
Damping coefficient, c	12	N·s/m
Mass of mover, m	1.024	kg

Based on (22) and (26), the piston stroke can be calculated by

$$\begin{aligned}\hat{x} = \hat{x}_1 &= \frac{1}{k_i}\left(\int u dt - R\int i dt - Li\right) \\ &= \frac{1}{k_i}\left(\frac{\hat{u}_2}{\omega} - \frac{R\hat{i}_2}{\omega} - L\hat{i}_1\right).\end{aligned} \tag{27}$$

This calculation method does not involve pure integration, which avoids those problems arising therefrom. At the same time, all voltage and current signals in the formula are processed by SO-SOGI, which reduces the dc offset and high-frequency burrs in the sampling process. Besides, SO-SOGI will not produce phase shift or amplitude change for the target signal of corresponding frequency in the process of filtering the signal. Thus, this calculation method can effectively improve the accuracy of stroke signal calculation. Similarly, the orthogonal signal x_2 of the stroke signal used in (18) in Section III-A can be obtained as follows:

$$\hat{x}_2 = \frac{dx}{\omega dt} = \frac{1}{k_i}\left(\frac{\hat{u}_1}{\omega} - \frac{R\hat{i}_1}{\omega} - L\hat{i}_2\right). \tag{28}$$

The method of calculation obtained from (27) and (28) is shown in Fig. 6.

V. SIMULATION AND EXPERIMENTS

A. Simulation and Analysis

The resonant frequency tracking control method of LOM based on CDC is simulated in this section, whose control block diagram is shown in Fig. 7. Specific parameters are given in Table I. In order to illustrate the effectiveness and the superiority of the proposed method, the traditional RFTC with SOGI based on virtual coordinate transformation method [12] is also carried on this article.

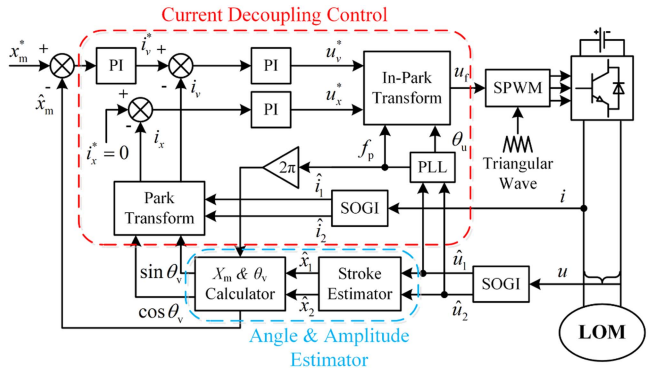

Fig. 7. Structure diagram of the LOM control system.

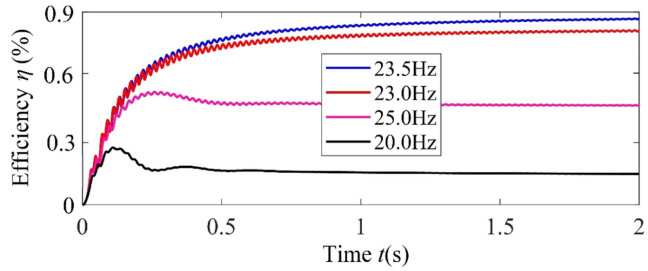

Fig. 8. Simulation results of motor operating efficiency at different frequencies.

First, simulation calculations should be conducted on the operational efficiency of LOM to verify the theoretical analysis mentioned in this article. Due to the complex characteristics of the cylinder and gas load, it is difficult to accurately obtain their input power and output power. Therefore, the operating efficiency of the electromagnetic part of the motor is mainly calculated here. The input electrical energy of the motor is obtained by integrating the product of motor voltage and current, and the mechanical energy output of the motor is obtained by integrating the product of motor thrust and piston speed. The ratio of the abovementioned two is the real-time power of the system. The power simulation results at different frequencies are shown in Fig. 8.

As shown in Fig. 8, when LOM operates at its resonant frequency of 23.5 Hz, its operating efficiency is the highest, about 86%. When the driving frequency of the motor is far away from the resonant frequency, regardless of whether the frequency increases or decreases, the operating efficiency of the motor will decrease. The change in driving frequency has a significant impact on the efficiency of the system operation. When the frequency error is 2.5 Hz, i.e., the driving frequency is 20.0 Hz, the efficiency of the motor operation is only about 15%. Therefore, it is essential to ensure that the motor always operates at the highest efficiency operating point, which is the resonant frequency.

The starting performance under load is shown in Fig. 9. As seen from this picture, the LOM starts up with piston amplitude of 5 mm. Fig. 9(a) and (c) show current and velocity during the starting. It is observed that, once the motor reaches steady state, the current and piston velocity of LOM are in phase under the proposed control algorithm. It is seen that the simulation results are consistent with related theoretical analysis.

During the starting process, the current component i_q increases rapidly and then remains stable, while the current component I_x remains 0 after adjustment. The simulation results show that the current vector decomposition system has a good control effect, and components are almost free of noise and harmonic interference. The current loop has both dynamic response speed and stability.

According to [11], the operating efficiency of LOM can be reflected approximately by observing the change of the driving frequency of the system. Comparing the driving frequency changes of the two control algorithms in the starting, the CDC algorithm has faster frequency response, better tracking performance, and almost no overshoot, which means the LOM has higher operation efficiency under the control algorithm.

The piston position signal during the starting is given in Fig. 9(b). It is seen that, after about 0.5 s, the piston amplitude reaches the given value of 5 mm. The amplitude response is fast without steady-state error. The I_x and I_v during startup is given in Fig. 9(d). It is known that, during the starting, the I_v rises rapidly with short overshoot, and reaches stable very quickly, while the I_x remains 0 by the quick adjustment based on the proposed method.

Fig. 9(e) and (f) show the comparison of the CDC and traditional RFTC algorithm with SOGI. The CDC completes the decoupling control of the system, thus avoiding the interaction between the parameters. Meanwhile, the piston amplitude and driving frequency are adjusted by controlling the current component. These characteristics make CDC get faster response speed than traditional control methods. As seen from Fig. 9, it is known that the CDC has faster frequency response, better tracking ability, and little overshoot during the startup process, which proves that the LOM has better drive performance under the CDC.

At the beginning, the LOM cannot work at its highest efficiency under the initial driving frequency. Meanwhile, the calculated current component is not completely accurate because the PLL has not completed the tracking of frequency and phase. Then, once the PLL approaches the frequency and phase synchronization, the frequency will rise from 20 Hz to about 23.5 Hz through the adjustment of the CDC. And the piston amplitude will finally reach the given value of 5 mm.

It can be observed in Fig. 9 that the amplitude and frequency response of CDC takes about 0.5 s during the starting process, which is significantly less than about 1.3 s of ASCP method. The dynamic response speed is consistent with related theoretical analysis. The better amplitude response of the CDC improves the maneuverability and flexibility of the LOM, which makes the control system safer and more reliable. At the same time, even though both control methods can maintain the highest operating efficiency under steady state, the better tracking performance of the CDC can improve the operating efficiency of the LOM in the whole startup process.

Fig. 10 shows a simulation comparison between CDC and traditional RFTC algorithm with SOGI during the loading process. The LOM load is the gas in the cylinder, making it difficult to

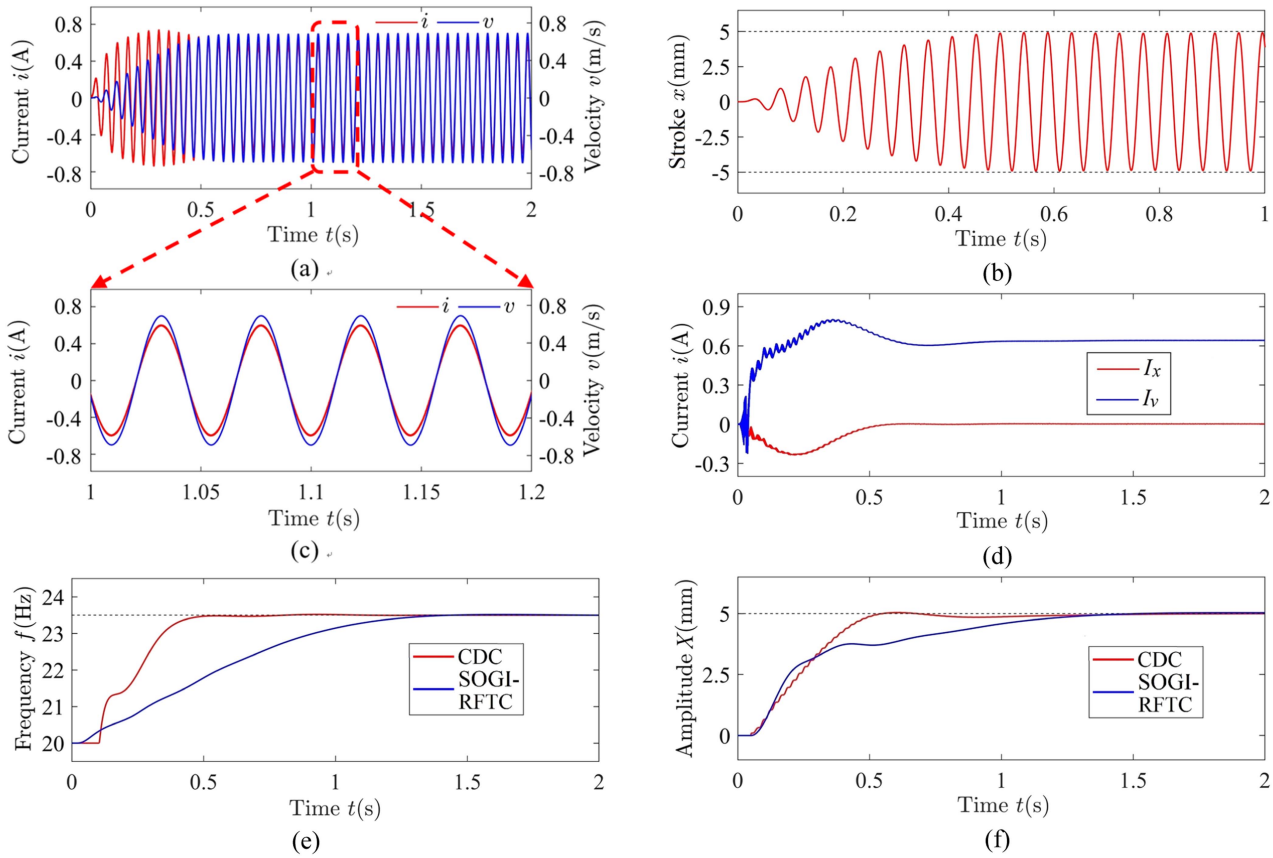

Fig. 9. Simulation results of loaded starting up. (a) Motor current i and piston speed v. (b) Piston stroke signal x. (c) Extended view of (a). (d) Current component I_x and I_v. (e) Frequency comparison. (f) Amplitude comparison.

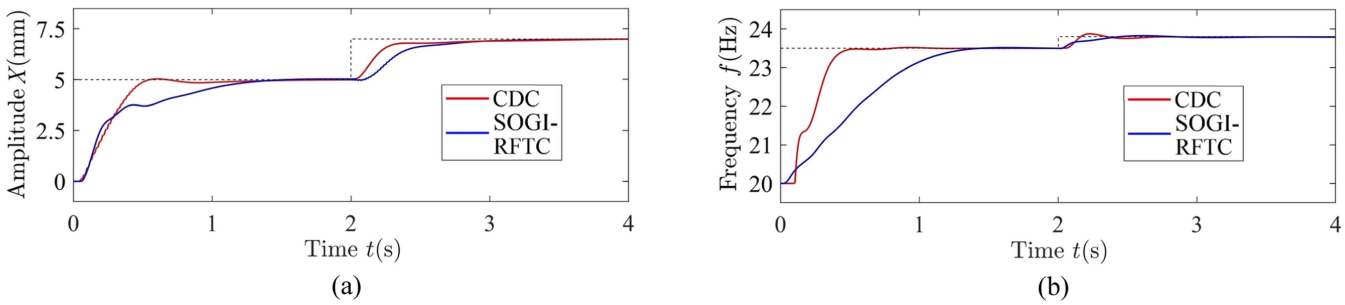

Fig. 10. Simulation results of changing piston amplitude. (a) Amplitude comparison. (b) Frequency comparison.

individually change its properties and parameters. Therefore, the loading and unloading of LOM is mainly achieved by changing the piston amplitude, and during this process, the parameters of the gas force load will also change accordingly. When the piston amplitude is changed from 5 to 7 mm, the gas load of the cylinder is also changed so that the equivalent elastic coefficient k and equivalent damping coefficient c will increase. And the increment of k would result in the rising resonant frequency of the drive system. Fig. 10(a) and (b) show the amplitude and frequency responses of the CDC and the traditional RFTC method with SOGI, respectively, when the piston amplitude changes. The piston amplitude rises rapidly to the given value of 7 mm under the control of algorithms, and the frequency rises up to the new resonance frequency of about 23.8 Hz. It can be observed that the amplitude and frequency responses of the CDC are faster than those of the traditional RFTC method with SOGI.

B. Experiments and Analysis

The experiment platform is shown in Fig. 11. And the hardware structure of LOM driver is shown in Fig. 12, which mainly consists of the prototyped LOM, the stroke sensor of Soway SDVG20-50A-V2-CFP LVDT, the Hall voltage sensor of CHV-50P/5mA/25mA, the Hall current sensor of LA-50P/5mA/25mA, and the inverter with the microprogrammed control unit (MCU) of STM32F407. The inverter communicates

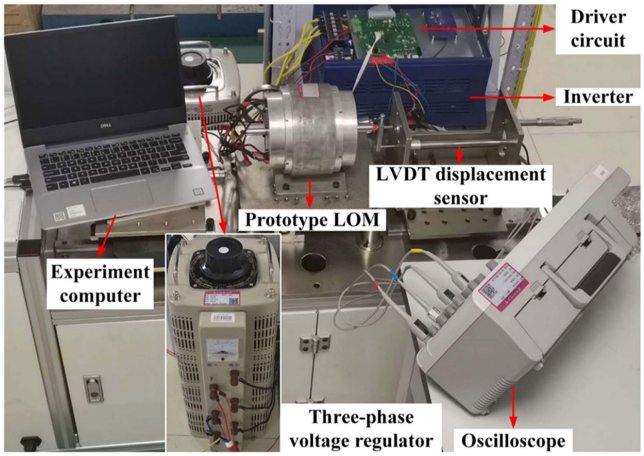

Fig. 11. Experiment platform.

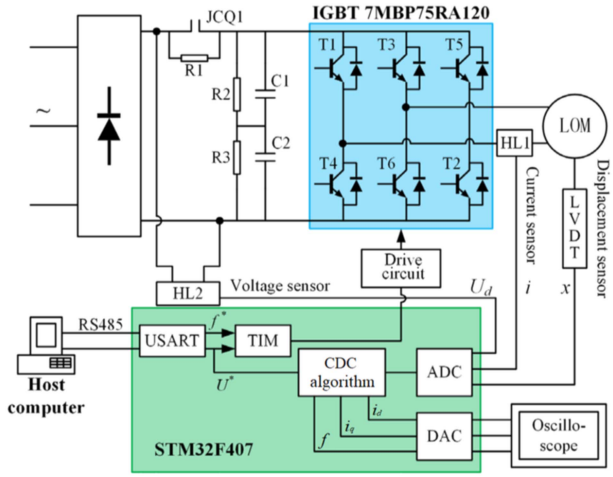

Fig. 12. Hardware structure of the LOM drive system.

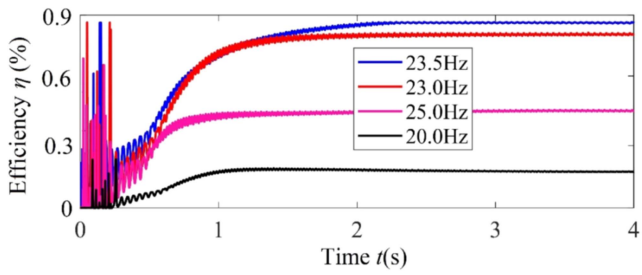

Fig. 13. Experimental results of motor operating efficiency at different frequencies.

with the host computer through the RS485 transceiver. In the MCU, the fundamental voltage in SPWM, the detected current and stroke signals are used by the CDC to complete decoupling control of current, and then adjust the operation of the LOM. The calculated values are converted from digital signals to analog ones by DAC peripherals as observed from an oscilloscope.

The experimental calculation results of motor efficiency changes at different frequencies are shown in Fig. 13. Similarly, the integration method is used to separately calculate the input

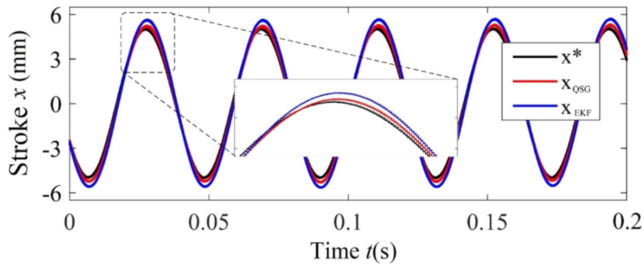

Fig. 14. Experimental comparison of position observation.

electrical energy and output mechanical energy of the motor, and then divide them to obtain the operating power of the motor. During the motor startup process, the operating condition of the motor and the voltage and current signals are relatively unstable. Due to the fact that the motor has not yet fully entered normal operating mode, the motor is not in a resonant state during the startup process, so the electromagnetic thrust does not fully perform positive work in each cycle. Therefore, the total input and output power are in a state of drastic fluctuations, and the calculated operating efficiency is also unstable. After the system runs stably, the calculated efficiency of the motor at that certain frequency can be obtained. As shown in Fig. 13, the motor has the highest operating efficiency at a driving frequency of 23.5 Hz, which is about 87%. When the driving frequency is higher or lower than the resonant frequency, its operating efficiency will significantly decrease. The experimental results are basically consistent with the simulation results.

The experimental results of position observation based on voltage and current components with SOGI proposed in this article are shown in Fig. 14. As seen from this picture, the center frequency of SOGI is the driving frequency of the system. The closed-loop gain coefficient in SOGI is configured as $k = 1.414$, and the corresponding bandwidth is 23.5 Hz. The result by observation method is given as x_{QSG}, the traditional open-loop back EMF method is x_{EKF}, and the actual stroke given by the sensor is $x*$. The accuracy of the position signal obtained by this observation method has been significantly improved compared to traditional algorithms, and its amplitude and phase errors have been reduced. The experimental results have fully demonstrated the effectiveness and superiority of the position observation algorithm.

Next, the CDC algorithm proposed in this article will be validated under different operating conditions. During the experiment, the PI parameters for i_{d} and i_{q} control are: $K_{\mathrm{p\_i}} = 0.24$, $K_{\mathrm{i\_i}} = 1.1$; the PI parameters for amplitude control are $K_{\mathrm{p\_x}} = 0.14$ and $K_{\mathrm{i\_x}} = 0.55$; the closed-loop gain of SOGI used in PLL is $k = 1.414$, and the PI parameters for PLL are $K_{\mathrm{p}\_\theta} = 55$, $K_{\mathrm{i}\_\theta} = 900$.

The variation of various parameters of LOM under the control of CDC algorithm during the load startup process are shown in Fig. 15. In this experiment, the motor was started with load, and the initial driving frequency was set to 20 Hz, with a given piston amplitude of 5 mm. Fig. 15(a) shows the response of the motor drive frequency during the startup process. As shown in Fig. 15(a), the driving frequency is adjusted to the resonant

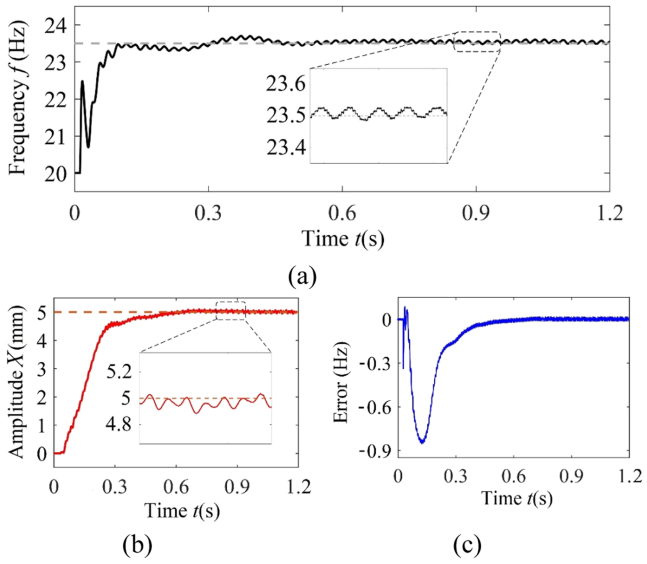

Fig. 15. Experimental results of loaded starting up. (a) Frequency adjustment. (b) Piston stroke amplitude response. (c) PLL controller error change.

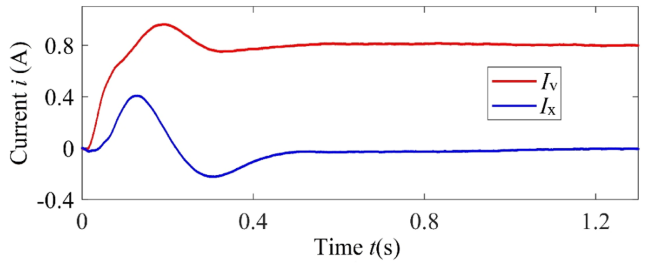

Fig. 16. Experimental results of orthogonal current component during loaded starting up.

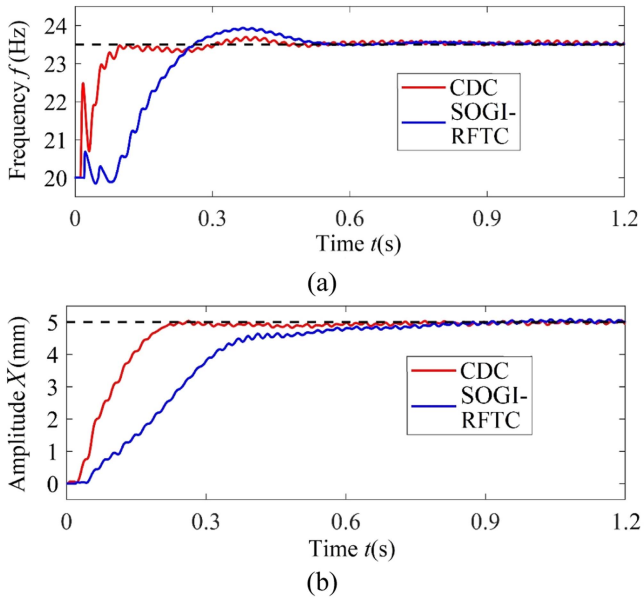

Fig. 17. Experimental comparison of loaded start up. (a) Frequency adjustment comparison. (b) Piston stroke amplitude response comparison.

frequency of 23.5 Hz after approximately 0.15 s. Subsequently, after a very slight fluctuation, the driving frequency remained basically stable. During steady-state operation, the motor drive frequency is also relatively stable, with a fluctuation amplitude less than 0.1 Hz. Fig. 15(b) shows the response of piston amplitude during the start-up process. During the startup process, the piston amplitude reaches the given value of 5 mm after about 0.6 s, with a fast response speed and no overshoot. At the same time, the effect of amplitude control in steady-state is also relatively ideal, with relatively small fluctuations of about 0.1 mm. The frequency error of the PLL controller during the startup process is shown in Fig. 15(c). It can be seen that consistent with the theoretical analysis in Section II-C, the PI controller in PLL plays a good role in frequency regulation. After about 0.5 s of error, it is adjusted to 0 and maintained stable during subsequent operation.

As shown in Fig. 16, the changes in the two current components during the startup process. It can be seen that after the motor starts, the current component I_v rises to about 0.8 A, while the current component I_x fluctuates back to 0. The overall adjustment process takes about 0.5 s, and the changes in the current component throughout the process are relatively smooth.

To verify the advantages of the proposed algorithm in response speed, a startup experiment was conducted on the traditional RFTC algorithm with SOGI under the same conditions. Fig. 17(a) shows the experimental comparison of amplitude response between CDC algorithm and RFTC algorithm with SOGI under transient conditions, and Fig. 17(b) shows the experimental comparison of frequency response between these two control algorithms. As shown in these figures, the CDC algorithm has significantly better speed than the traditional RFTC algorithm with SOGI in both frequency and amplitude responses. Among them, the frequency adjustment takes about 25% of the latter, while the amplitude adjustment takes about 30% of the latter.

Subsequently, conduct experiments on the motor loading process. As shown in Fig. 18, under the stable operation of the motor piston with an amplitude of 5 mm, increase the given amplitude value to 7 mm. Fig. 18(a) shows the variation of driving frequency during the loading process. When the amplitude of the piston increases, due to changes in the nature of the gas load, the resonant frequency of the motor increases from 23.5 Hz to approximately 23.9 Hz. As the gas pressure and the amount of gas in the cylinder also need time to be changed, there will be a process of parameters changing. Therefore, the frequency response speed under this operating condition is slightly slower than the starting process of the motor. It can be seen, after the amplitude changes, the frequency rises to the new resonant frequency of 23.9 Hz after about 0.7 s. The variation of piston amplitude during the entire adjustment process is shown in Fig. 18(b). When the given amplitude value changes, the system only takes about 0.2 s to complete the amplitude response, adjusting the piston amplitude to about 7 mm. Subsequently, it remained stable after slight fluctuations, and the overall switching process was relatively smooth. The variation of frequency error in the controller during the loading process is shown in

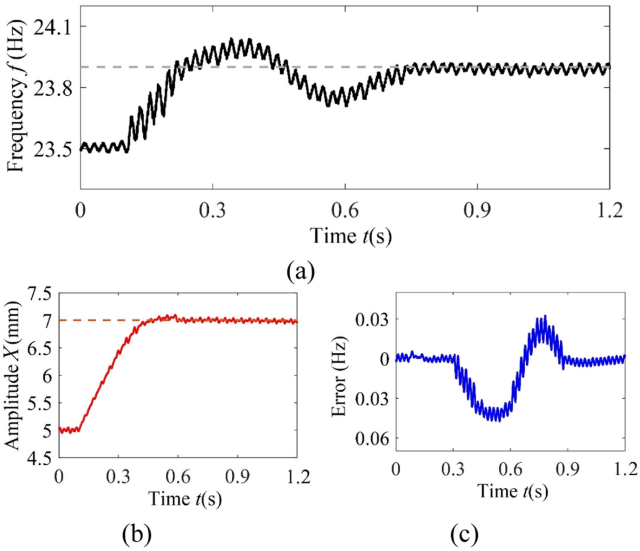

Fig. 18. Experimental results of load increasing condition. (a) Frequency adjustment. (b) Piston stroke amplitude response. (c) PLL controller error change.

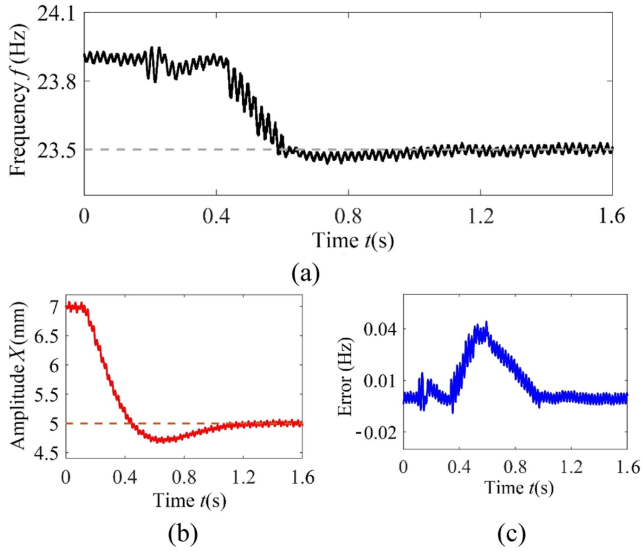

Fig. 20. Experimental results of load decreasing condition. (a) Frequency adjustment. (b) Piston stroke amplitude response. (c) PLL controller error change.

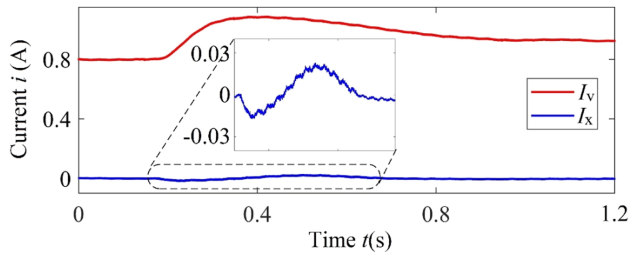

Fig. 19. Experimental results of orthogonal current component during load increasing condition.

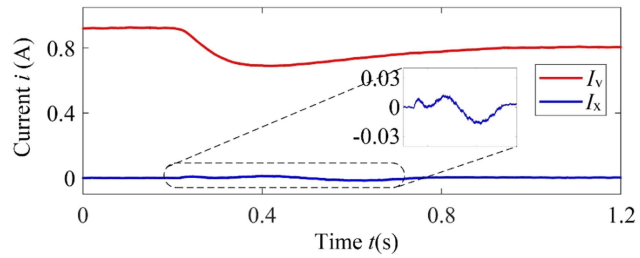

Fig. 21. Experimental results of orthogonal current component during load decreasing condition.

Fig. 18(c). Within approximately 0.1 s after switching, due to the time required for the gas load to rise, the frequency error is still basically 0. After about 0.6 s of adjustment, the PLL error returned to 0 and remained basically stable.

The variation of the two current components during the loading process is shown in Fig. 19. As shown in the figure, during the variation of piston amplitude, the current component I_v temporarily rises to about 1.1 A and then stabilizes to about 0.95 A. The current component I_x remains stable after slight fluctuations. The overall adjustment process takes about 0.7 s, and its adjustment process is basically consistent with the frequency response situation.

Finally, conduct experiments on the process of motor load reduction. In the steady state with a piston amplitude of 7 mm, the given amplitude value was modified to 5 mm to simulate the unloading condition. The experimental results are shown in Figs. 20 and 21. Fig. 20(a) shows the adjustment process of driving frequency under transient conditions. It can be seen that after a fluctuation of about 0.4 s, the driving frequency of the motor decreased from 23.9 Hz to about 23.5 Hz and then remained stable for the following time. Fig. 20(b) shows the response of piston amplitude. During the load reduction process, as the piston amplitude decreases, the gas force load also continuously decreases. Therefore, as shown in this figure, there is an overshoot of approximately 0.2 mm in the amplitude adjustment process, which will not affect the normal operation of the motor. After giving the variable load command, the piston amplitude reaches the given value of 5 mm in about 1.0 s, which takes a slightly longer time but the overall adjustment process is relatively stable. The amplitude control can effectively complete its function. Fig. 20(c) shows the variation of PLL controller frequency error during the adjustment process. Under transient conditions, after approximately 1.0 s of adjustment, the controller error returns to 0 and remains stable.

Fig. 21 shows the variation of the current component during the load shedding process. Similar to the loading condition, after the command is issued, the current component I_v decreases to about 0.68 A, then gradually rises to about 0.8 A and remains stable. At the same time, the current component I_x remains at 0 after slight fluctuations. The overall adjustment process takes about 0.8 s, and the current inner loop can effectively achieve the function of current control.

The experimental results fully demonstrate the advantages of the dynamic response. Compared to the traditional RFTC control strategy, the response speed frequency and piston amplitude control are significantly improved by the CDC method. It is

worth noting that the frequency jitter of the CDC algorithm in steady-state is slightly larger than that of RFTC. This is mainly due to the fact that PLL in the algorithm proposed in this article has not been specially designed for the characteristics of LOM. In addition, the double-layer frequency adjustment mechanism of PLL-i_{d} in the algorithm slightly reduces the stability of frequency control. Nevertheless, the experimental results indicate that the frequency jitter phenomenon of the CDC algorithm in steady-state is still very slight and will not affect the operation of the motor.

VI. Conclusion

In this article, a fast efficiency optimization control method based on orthogonal current phasor model for the LOM is proposed. The operation efficiency of the system is improved by decomposing the current along the direction of the piston speed and optimizing the current composition. Moreover, the piston amplitude is adjusted by controlling the thrust of the LOM. The effectiveness of the control algorithm is verified by both simulation and experimental results. Compared with the traditional algorithms, the proposed CDC has benefited from faster dynamic response on piston amplitude response and quicker convergence on frequency tracking, and so on.

References

[1] X. Li, W. Xu, C. Ye, and I. Boldea, "Comparative study of transversal-flux permanent magnetic linear oscillatory machines for compressor," *IEEE Trans. Ind. Electron.*, vol. 65, no. 9, pp. 7437–7446, Sep. 2018.

[2] X. Xue, K. W. E. Cheng, and Z. Zhang, "Model, analysis, and application of tubular linear switched reluctance actuator for linear compressors," *IEEE Trans. Ind. Electron.*, vol. 65, no. 12, pp. 9863–9872, Dec. 2018.

[3] X. Li, W. Xu, C. Ye, and J. Zhu, "Novel hybrid-flux-path moving-iron linear oscillatory machine with magnets on stator," *IEEE Trans. Magn.*, vol. 53, no. 11, Nov. 2017, Art. no. 8210405.

[4] K. Liang, "A review of linear compressors for refrigeration," *Int. J. Refrigeration*, vol. 84, pp. 253–273, Dec. 2017.

[5] W. Xu, X. Li, J. Zhu, and Q. Wang, "3-D modeling and testing of a stator-magnet transverse-flux linear oscillatory machine for direct compressor drive," *IEEE Trans. Ind. Electron.*, vol. 68, no. 9, pp. 8474–8486, Sep. 2021.

[6] H. Kim et al., "An experimental and numerical study on dynamic characteristic of linear compressor in refrigeration system," *Int. J. Refrigeration*, vol. 32, no. 7, pp. 1536–1543, Nov. 2009.

[7] Y. Zhang, Q. Lu, M. Yu, and Y. Ye, "A novel transverse-flux moving-magnet linear oscillatory actuator," *IEEE Trans. Magn.*, vol. 48, no. 5, pp. 1856–1862, May 2012.

[8] C. Pompermaier, K. Kalluf, A. Zambonetti, M. V. Ferreira da Luz, and I. Boldea, "Small linear PM oscillatory motor: Magnetic circuit modeling corrected by axisymmetric 2-D FEM and experimental characterization," *IEEE Trans. Ind. Electron.*, vol. 59, no. 3, pp. 1389–1396, Mar. 2012.

[9] T.-W. Chun, J.-R. Ann, J.-Y. Yoo, and C.-W. Lee, "Analysis and control for linear compressor system driven by PWM inverter," in *Proc. Annu. Conf. IEEE Ind. Electron. Soc.*, 2004, vol. 1, pp. 263–267.

[10] C. Demoulias and K. Gouramanis, "Voltage multiple-zero-crossings at buses feeding large triac-controlled loads," *IEEE Trans. Ind. Electron.*, vol. 54, no. 5, pp. 2853–2863, Oct. 2007.

[11] T.-W. Chun, J.-R. Ahn, H.-H. Lee, H.-G. Kim, and E.-C. Nho, "A novel strategy of efficiency control for a linear compressor system driven by a PWM inverter," *IEEE Trans. Ind. Electron.*, vol. 55, no. 1, pp. 296–301, Jan. 2008.

[12] T. Zhang and H. Yu, "A novel strategy of resonant frequency tracking control for linear compressor," in *Proc. Int. Conf. Elect. Mach. Syst.*, 2017, pp. 1–6.

[13] W. Xu et al., "A novel resonant frequency tracking control for linear compressor based on MRAS method," *CES Trans. Elect. Mach. Syst.*, vol. 4, no. 3, pp. 227–236, Sep. 2020.

[14] W. Xu, Q. Wang, Y. Liu, X. Li, and K. Liao, "Adaptive full-order stroke observer for sensorless resonant frequency tracking control of linear oscillatory machines," *IEEE Trans. Ind. Electron.*, vol. 69, no. 2, pp. 1310–1321, Feb. 2022.

[15] J. Latham, M. L. McIntyre, and M. Mohebbi, "Nonlinear adaptive current control for linear vapor compressors," in *Proc. IEEE Int. Conf. Automat. Sci. Eng.*, 2016, pp. 1257–1262.

[16] J. Latham, M. L. McIntyre, and M. Mohebbi, "Sensorless resonance tracking and stroke control of a linear vapor compressor via nonlinear observers," *IEEE Trans. Ind. Electron.*, vol. 65, no. 5, pp. 3720–3729, May 2018.

[17] M. A. Akhtar and S. Saha, "An adaptive frequency-fixed second-order generalized integrator-quadrature signal generator using fractional-order conformal mapping-based approach," *IEEE Trans. Power Electron.*, vol. 35, no. 6, pp. 5548–5552, Jun. 2020.

[18] Z. Xin, X. Wang, Z. Qin, M. Lu, P. C. Loh, and F. Blaabjerg, "An improved second-order generalized integrator based quadrature signal generator," *IEEE Trans. Power Electron.*, vol. 31, no. 12, pp. 8068–8073, Dec. 2016.

[19] S. Golestan, J. M. Guerrero, F. Musavi, and J. C. Vasquez, "Single-phase frequency-locked loops: A comprehensive review," *IEEE Trans. Power Electron.*, vol. 34, no. 12, pp. 11791–11812, Dec. 2019.

Wei Xu (Fellow, IEEE) received the double B.E. and M.E. degrees from Tianjin University, Tianjin, China, in 2002 and 2005, respectively, and the Ph.D. degree from the Institute of Electrical Engineering, Chinese Academy of Sciences (IEECAS), Beijing, China, in 2008, respectively, all in electrical engineering.

From 2008 to 2012, he was a Postdoctoral Fellow with the University of Technology Sydney, a Vice Chancellor Research Fellow with the Royal Melbourne Institute of Technology, and a Japan Science Promotion Society Invitation Fellow with Meiji University, respectively. From October 2013 to December 2023, he was a Professor with Huazhong University of Science and Technology, China. Since January 2024, he has been a Professor with IEECAS. His research topics mainly focus on design and control for linear machines and drives.

Dr. Xu is the General Chair for the 2021 International Symposium on Linear Drives for Industry Applications (LDIA 2021) and the 2023 IEEE International Conference on Predictive Control of Electrical Drives and Power Electronics (PRECEDE 2023). He has been an Associate Editor for ten peer-reviewed IEEE journals, including the IEEE Transactions on Industrial Electronics, IEEE Transactions on Power Electronics, and so on. He is a Fellow of the Institute of Engineering and Technology (IET).

Yifan Gong is currently working toward the M.E. degree in electrical engineering with Huazhong University of Science and Technology, Wuhan, China.

His research interests include advanced control strategies on linear oscillatory machine.

Jian Ge (Member, IEEE) was born in Heilongjiang, China, in 1994. He received the B.E., M.E., and Ph.D. degrees in electrical engineering from Huazhong University of Science and Technology, Wuhan, China, in 2016, 2019, and 2022, respectively.

He is currently a Postdoctoral Researcher in electrical engineering with Huazhong University of Science and Technology. His research interests include induction machines, linear machines, and brushless doubly-fed machines.

Kaiju Liao received the Ph.D. degree in electrical engineering from Huazhong University of Science and Technology, Wuhan, China, in 2023.

He is currently a Postdoctoral Researcher in Electrical Engineering with the Institute of Electrical Engineering, Chinese Academy of Sciences, Beijing, China. His research interest is control for linear machine.

Guangyu Liao is currently working toward the M.E. degree in electrical engineering with Huazhong University of Science and Technology, Wuhan, China.

His research interests include electromagnetic design and theoretical analysis of novel permanent magnet linear machines.

Maoxin Zhang is currently working toward the Ph.D. degree in electrical engineering with the School of Electrical Engineering, Huazhong University of Science and Technology, Wuhan, China.

His research interests include linear machines and brushless doubly-fed machines.

Ion Boldea (Life Fellow, IEEE) received the M.S. and Ph.D. degrees in electrical engineering from the University Politehnica of Timisoara, Timisoara, Romania, in 1967 and 1973, respectively.

He is currently a Full Professor with the University Politehnica of Timisoara. He has authored or coauthored research papers extensively (291 papers, 5395 citations, H index: 40 in Web of Science) in linear and rotary electric machines, drives, and MAGLEVs, and numerous books, with 6000 entrances in libraries worldwide.

Dr. Boldea was the recipient of the 2015 IEEE Nikola Tesla Award.